1993MNRAS.265..250D

Mon. Not. R. Astron. Soc. **265**, 250–256 (1993)

A family of potential–density pairs for spherical galaxies and bulges

Walter Dehnen
Landessternwarte Königstuhl, D 69117 Heidelberg, Germany

Accepted 1993 June 18. Received 1993 June 18; in original form 1993 May 13

ABSTRACT

A family of spherical potential–density pairs is presented. The densities are proportional to r^{-4} at large radii and diverge in the centre as $r^{-\gamma}$ with $0 \le \gamma < 3$. The models of Jaffe and Hernquist are included as special cases. The gravitational potential is analytical for all γ. For specific values of γ, most of the intrinsic and projected properties, such as distribution function, surface density and projected velocity dispersion, can be expressed in terms of elementary functions. A comparison to the de Vaucouleurs $R^{1/4}$-profile shows that the model with $\gamma = 3/2$ most closely resembles it in both surface density and distribution function. This particular model is completely analytical, and thus it is the best analytical approximation of the $R^{1/4}$-model known so far.

Key words: celestial mechanics, stellar dynamics – galaxies: elliptical and lenticular, cD – galaxies: kinematics and dynamics – galaxies: photometry – galaxies: structure.

1 INTRODUCTION

The observed luminosity profiles of ellipticals and bulges are often well described by the empirical formula $I \propto \exp(-\text{constant} \times R^{1/4})$ (de Vaucouleurs 1948). While widely used to derive global quantities for observed galaxies, such as effective radius and effective surface brightness, this profile is less useful for detailed modelling, mainly because it cannot be deprojected to yield the spatial density or the gravitational potential analytically. Furthermore, its logarithmic slope, $\mathrm{d}(\ln I)/\mathrm{d}(\ln R)$, vanishes in the centre. This is certainly not in contradiction with most (low-resolution) observations, but recent high-resolution imaging indicates that the majority of galaxies may have a constant logarithmic slope almost all the way into the centre (e.g. Lauer et al. 1992; Crane & Stiavelli 1993).

For these reasons, one is interested in simple models for the spatial stellar density, which in projection resemble de Vaucouleurs' profile in the outer parts, but not necessarily in the centre. Two such models are those introduced by Jaffe (1983) and Hernquist (1990), which have central stellar densities proportional to r^{-2} and r^{-1}, resulting in central surface densities proportional to R^{-1} and $\ln R^{-1}$, respectively. These two models can be generalized to a family of density profiles with different central slopes:

$$\rho(r) = \frac{(3-\gamma)M}{4\pi} \frac{a}{r^{\gamma}(r+a)^{4-\gamma}}, \qquad (1)$$

where a is a scaling radius and M the total mass. In the centre these mass distributions are proportional to $r^{-\gamma}$, so that the models by Jaffe and Hernquist correspond to $\gamma = 2$ and 1, respectively. The parameter γ is restricted to the interval $[0, 3)$. Thus equation (1) represents mass models with central density cusps that are shallower then r^{-3} or even asymptotically flat (r^0).

Real galaxies and bulges are hardly spherical. However, the models that result from equation (1) by replacing the radius r by an axisymmetric or triaxial radius $m = \sqrt{x^2 + (y/q_2)^2 + (z/q_3)^2}$ are similar to the spherical models in some important properties: e.g. surface brightness, cumulative mass and differential energy distribution $N(E)$. Also, the typical behaviours of the dynamical quantities at small and large radii are the same.

This paper is organized as follows. Section 2 investigates the properties of the models and their changes with the parameter γ. The surface densities and self-consistent distribution functions for different values of γ are compared to those of de Vaucouleurs' $R^{1/4}$-model in Section 3. Finally, Section 4 sums up and concludes.

2 CHARACTERISTICS OF THE MODELS

In this section the intrinsic and projected properties for the family of models of equation (1) are analysed. More explicit equations for $\gamma = 0$ and 3/2 are given in Appendix A.

2.1 Intrinsic properties

2.1.1 *Potential and velocity moments*

The potential that corresponds to the density of equation (1) via Poisson's equation is

© Royal Astronomical Society • Provided by the NASA Astrophysics Data System

Downloaded from https://academic.oup.com/mnras/article/265/1/250/975506 by guest on 20 August 2022

1993MNRAS.265..250D

$$\Phi(r) = \frac{GM}{a} \times \begin{cases} -\dfrac{1}{2-\gamma}\left[1-\left(\dfrac{r}{r+a}\right)^{2-\gamma}\right] & \gamma \neq 2 \\ \ln\dfrac{r}{r+a} & \gamma = 2. \end{cases} \quad (2)$$

For $\gamma<2$ it has a finite central value of $(2-\gamma)^{-1}GM/a$.

The cumulative mass, half-mass radius and circular velocity are

$$M(r) = M\left(\frac{r}{r+a}\right)^{3-\gamma}, \quad (3)$$

$$r_{1/2} = a\left(2^{1/(3-\gamma)}-1\right)^{-1}, \quad (4)$$

$$v_c^2(r) = \frac{GM\,r^{2-\gamma}}{(r+a)^{3-\gamma}}. \quad (5)$$

The intrinsic velocity dispersion is connected to potential and density by the Jeans equation (cf. Binney & Tremaine 1987, hereafter BT). For the isotropic case the solution is given by

$$\overline{v_r^2}(r) = GM\,r^{\gamma}(r+a)^{4-\gamma}\int_r^{\infty}\frac{r'^{1-2\gamma}\,\mathrm{d}r'}{(r'+a)^{7-2\gamma}}, \quad (6)$$

which can be calculated analytically only if 4γ is an integer. At small radii, $\overline{v_r^2} \propto r^{2-\gamma}$ for $\gamma \geq 1$ and $\overline{v_r^2} \propto r^{\gamma}$ for $\gamma \leq 1$. Thus both v_c^2 and $\overline{v_r^2}$ diverge in the centre for models with $\gamma > 2$, while they are finite for Jaffe's model ($\gamma = 2$), which has an isothermal cusp. For $\gamma < 2$, not only the circular velocity but also the isotropic velocity dispersion declines to zero in the centre, except for $\gamma = 0$, where $\overline{v_r^2}(0) = GM/30a$.

The density can be expressed in terms of the potential. For this purpose it is useful to define $y \equiv r/(r+a)$ and the dimensionless positive potential $\Psi \equiv -\Phi(GM/a)^{-1}$. Then

$$y = y(\Psi) = \begin{cases} [1-(2-\gamma)\Psi]^{1/(2-\gamma)} & \gamma \neq 2 \\ \mathrm{e}^{-\Psi} & \gamma = 2, \end{cases} \quad (7)$$

and

$$\rho(\Phi) = \frac{(3-\gamma)M}{4\pi a^3}\,\frac{(1-y)^4}{y^{\gamma}}. \quad (8)$$

The dimensionless binding energy (defined by $\mathscr{E} \equiv -E(GM/a)^{-1}$) of the circular orbit at radius r_c is, for $\gamma \neq 2$,

$$\mathscr{E}_c = \frac{1}{2-\gamma} - \frac{4-\gamma}{2(2-\gamma)}y_c^{2-\gamma} + \frac{1}{2}y_c^{3-\gamma} \quad (9)$$

with $y_c \equiv r_c/(r_c+a)$. For $\gamma = 0, 1, \frac{3}{2}, \frac{9}{4}, \frac{7}{3}$ or $\frac{5}{2}$, equation (9) is of order four or less and can be solved analytically for y_c. This in turn yields the angular momentum of the circular orbit as an analytical function of energy:

$$L_c^2(\mathscr{E}) = GMa\,y_c^{4-\gamma}/(1-y_c). \quad (10)$$

2.1.2 *Distribution functions*

The distribution function (hereafter DF) of the isotropic models can be calculated using an Abel transform (cf. BT), which gives

$$f(\mathscr{E}) = \frac{(3-\gamma)\,M}{2(2\pi^2 GMa)^{3/2}}\int_0^{\mathscr{E}}\frac{(1-y)^2[\gamma+2y+(4-\gamma)y^2]}{y^{4-\gamma}\sqrt{\mathscr{E}-\Psi}}\mathrm{d}\Psi \quad (11)$$

where $y = y(\Psi)$ is given in equation (7). For $\gamma \neq 2$, $f(\mathscr{E})$ can generally be expressed in terms of hypergeometric series, which reduce to elementary functions for integer or half-integer values of $(2-\gamma)^{-1}$, e.g. for $\gamma = 0, 1, \frac{3}{2}, \frac{7}{4}, \frac{9}{4}, \frac{5}{2}$. At low binding energies $f(\mathscr{E})$ falls off as $\mathscr{E}^{5/2}$. At high binding energies $f(\mathscr{E})$ diverges like

$$f(\mathscr{E} \to \Psi(0)) \propto \begin{cases} [\Psi(0)-\mathscr{E}]^{-1} & \gamma = 0 \\ [\Psi(0)-\mathscr{E}]^{-(6-\gamma)/2(2-\gamma)} & 0<\gamma<2 \\ \mathrm{e}^{2\mathscr{E}} & \gamma = 2 \\ \mathscr{E}^{(6-\gamma)/2(\gamma-2)} & 2<\gamma<3, \end{cases} \quad (12)$$

but this is no difficulty since there is vanishingly little mass at these energies (see below). The density of states at a given energy can be calculated using a formula given by BT; the result is

$$g(\mathscr{E}) = 16\pi^2\sqrt{2GMa^5}\int_{\mathscr{E}}^{\Psi(0)}\frac{y^{\gamma+1}}{(1-y)^4}\sqrt{\Psi-\mathscr{E}}\,\mathrm{d}\Psi. \quad (13)$$

For the isotropic models, the differential energy distribution $\mathrm{d}M/\mathrm{d}\mathscr{E}$ is given by $N(\mathscr{E}) = f(\mathscr{E})g(\mathscr{E})$ (BT). For low binding energies it converges to $8a(3-\gamma)/5G$, while at high binding energies $N(\mathscr{E})$ goes smoothly to zero like

$$N(\mathscr{E} \to \Psi(0)) \propto \begin{cases} [\Psi(0)-\mathscr{E}] & \gamma = 0 \\ [\Psi(0)-\mathscr{E}]^{1/(2-\gamma)} & 0<\gamma<2 \\ \mathrm{e}^{-\mathscr{E}} & \gamma = 2 \\ \mathscr{E}^{1/(2-\gamma)} & 2<\gamma<3, \end{cases} \quad (14)$$

which means that the isotropic models have no stars at rest in the centre, in spite of the fact that $f(\mathscr{E})$ diverges there.

The DFs of Osipkov–Merritt type (Osipkov 1979; Merritt 1985), $f_{\mathrm{OM}}(Q)$ with $Q = \mathscr{E} - L^2/(2r_a^2 GMa)$, where r_a is the anisotropy radius, are given by

$$f_{\mathrm{OM}}(Q) = f(Q) + \frac{a^2}{r_a^2}\frac{(3-\gamma)\,M}{2(2\pi^2 GMa)^{3/2}} \times \int_0^{Q}\frac{(4-\gamma)y^{\gamma}-(3-\gamma)y^{\gamma-1}}{\sqrt{Q-\Psi}}\mathrm{d}\Psi, \quad (15)$$

where $f(Q)$ is given in equation (11) and $y = y(\Psi)$ of equation (7). These DFs can be calculated in the same manner as the isotropic DFs above.

2.2 Observables – projected properties

2.2.1 *The surface density*

The projected density $\Sigma(R) = 2\int_R^{\infty}\rho(r)r/\sqrt{r^2-R^2}\mathrm{d}r$ is expressible in terms of elementary functions for integer γ, or in terms of elliptic integrals for half-integer γ. However, the asymptotic behaviour can be inferred for the general case: at large radii, $\Sigma \propto R^{-3}$. In the centre, models with $\gamma > 1$ have $\Sigma \propto R^{1-\gamma}$. The Hernquist model ($\gamma = 1$) has logarithmically diverging central surface density. For models with $\gamma < 1$ the central surface density is finite with $\Sigma(0) = [(2-\gamma)(1-\gamma)\pi]^{-1}M/a^2$, and falls off from this value as $R^{1-\gamma}$. In Fig. 1 the surface density profiles and their logarithmic slopes are plotted; they are computed by numerical quadrature of a formula given in Appendix B. The models with $\gamma < 1$ have surface density profiles that flatten into the centre. Therefore, in spite of their intrinsically shallow density cusps, in projection these models all appear to have a core, and can hardly be distinguished from each other.

The cumulative surface density, which is defined by $S(R) = 2\pi\int_0^R \Sigma(R)R\,\mathrm{d}R$, can be written as

$$S(R) = M - (3-\gamma)Ma\int_R^{\infty}\frac{r^{1-\gamma}\sqrt{r^2-R^2}\,\mathrm{d}r}{(r+a)^{4-\gamma}}, \quad (16)$$

Downloaded from https://academic.oup.com/mnras/article/265/1/250/975506 by guest on 20 August 2022

© Royal Astronomical Society • Provided by the NASA Astrophysics Data System

1993MNRAS.265..250D

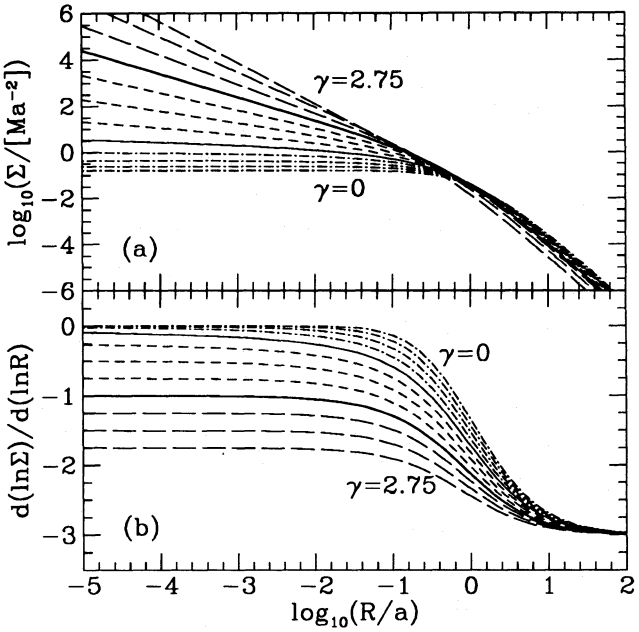

Figure 1. Surface density (a) and its logarithmic slope (b) for the mass models of equation (1). Dashed-dotted lines: $\gamma=0$, 0.25,0.5,0.75; the thin solid line: Hernquist's model ($\gamma=1$); dashed lines: $\gamma=1.25,1.5,1.75$; the thick solid line: Jaffe's model ($\gamma=2$); and long dashed lines: $\gamma=2.25,2.5,2.75$.

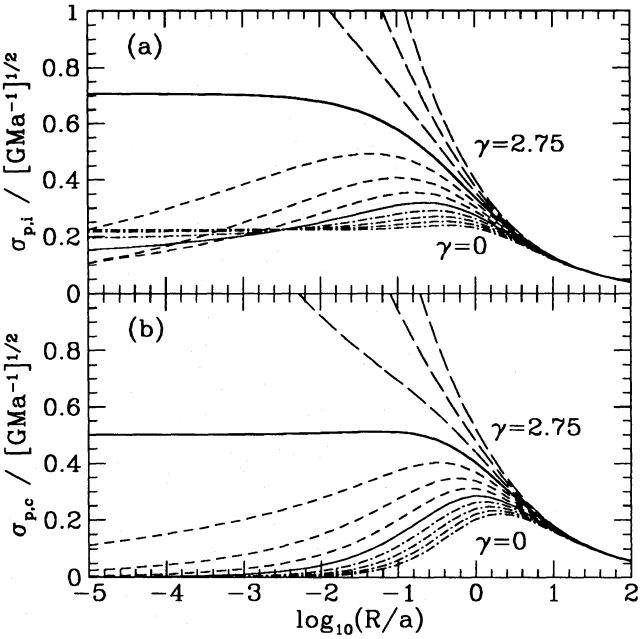

Figure 2. Profiles of the projected velocity dispersions of (a) isotropic and (b) circular models. The line styles are the same as in Fig. 1.

which again gives elementary functions for integer γ and elliptic integrals for half-integer γ. The effective radius, defined by $S(R_e)=M/2$, must generally be computed numerically. The ratio of effective to half-mass radius depends only slightly on γ. An approximation for $\gamma\le5/2$ is

$$\frac{R_e}{r_{1/2}}\approx0.7549-0.004\,39\gamma+0.003\,22\gamma^2 -0.001\,82\gamma^3\pm0.0007. \quad (17)$$

This ratio of $R_e/r_{1/2}\approx3/4$ seems to be relatively independent of the mass model. It is also found for models that have surface density profiles $\Sigma\propto\exp(-bR^{1/m})$ (Ciotti 1991). The relationship R_e/a follows from equations (4) and (17).

2.2.2 *Projected velocity dispersions*

The projected velocity dispersion for isotropic models (cf. BT) is

$$\sigma^2_{p,i}(R)=\frac{(3-\gamma)GM^2a^3}{2\pi\Sigma(R)}\int_R^\infty\frac{r^{1-2\gamma}}{(r+a)^{7-2\gamma}}\sqrt{r^2-R^2}\,\mathrm{d}r, \quad (18)$$

while for models containing only circular orbits it is

$$\sigma^2_{p,c}(R)=\frac{(3-\gamma)GM^2R^2a}{4\pi\Sigma(R)}\int_R^\infty\frac{r^{1-2\gamma}}{(r+a)^{7-2\gamma}}\frac{\mathrm{d}r}{\sqrt{r^2-R^2}}. \quad (19)$$

The integrals in equations (18) and (19) can be calculated analytically only if 4γ is an integer. However, it is possible to infer the asymptotic behaviour at small and large radii for all γ. In the outer envelope both dispersions decrease as in the Keplerian limit like $R^{-1/2}$. In the centre $\sigma^2_{p,c}$ behaves like $R^{2-\gamma}$ for $\gamma>1$, like $R^{3-2\gamma}$ for $1/2\le\gamma\le1$, and like R^2 for $\gamma<1/2$. The behaviour of the isotropic models at small radii is $\sigma^2_{p,i}\propto R^{2-\gamma}$ for $\gamma\ge3/2$ and $\sigma^2_{p,i}\propto R^{\gamma-1}$ for $1\le\gamma<3/2$, the Hernquist model has $\sigma_{p,i}\propto(\ln R)^{-1}$, and all models with $\gamma<1$ have a finite central projected velocity dispersion of $\sigma^2_{p,i}(0)=3(1-\gamma)/[4(3-2\gamma)(5-2\gamma)]GM/a$.

In Figs 2(a) and (b) the radial profiles of the projected velocity dispersion for isotropic and circular models are plotted; they are computed by numerically integrating formulæ given in Appendix B. As for the surface brightness, the radial profiles of velocity dispersion are rather similar for models with $\gamma\le1$ (see Fig. 2). Note that the projected isotropic velocity dispersion profiles of the models with $1\le\gamma<2$ go to zero in the very centre. This feature, however, will disappear under realistic observing conditions (even with little seeing), which can be demonstrated as follows. The dispersion is given as the quotient of the two projected moments $\Sigma\sigma^2_{p,i}$ and Σ, the first of which diverges in the centre as $R^{3-2\gamma}$ for $\gamma>3/2$ and goes to a constant for $\gamma\le3/2$, whereas Σ diverges more strongly (see above). Seeing will cut these singularities to finite values, which then result in a finite measured central velocity dispersion.

2.2.3 *Line-of-sight velocity profiles*

The integration of the distribution function over the two velocity components in the plane of the sky and subsequent integration along the line of sight result in the distribution of stars over line-of-sight velocities, which I will call the *velocity profile* (hereafter VP). When observing a stellar system, the VP is the function by which the stellar spectra are broadened, yielding the galaxy spectrum. Due to higher resolution of the data and improved deconvolution techniques, it is now possible to measure directly the VPs of elliptical galaxies (Franx & Illingworth 1988; Bender 1990; Rix & White 1992; van der Marel & Franx 1993). In the case of the VPs in spherical systems with general anisotropic DFs, $f(\mathscr{E},L^2)$, there is no way

Downloaded from https://academic.oup.com/mnras/article/265/1/250/975506 by guest on 20 August 2022

© Royal Astronomical Society • Provided by the NASA Astrophysics Data System

1993MNRAS.265..250D

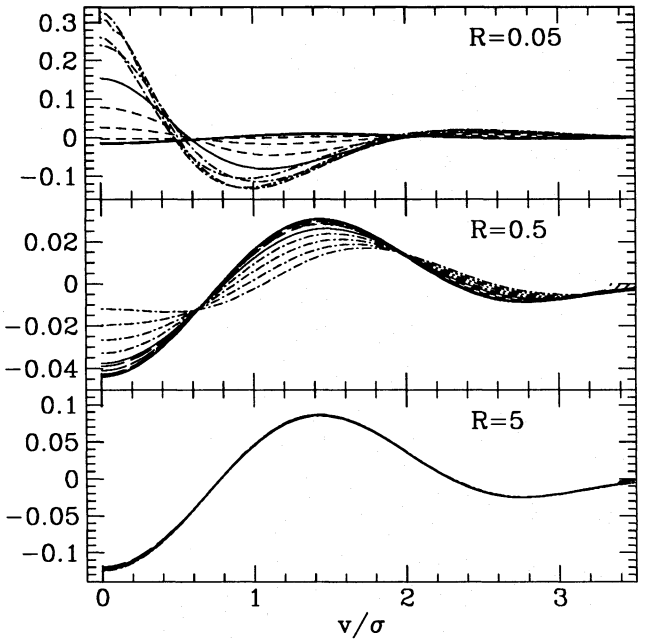

Figure 3. Line-of-sight velocity profiles of the isotropic models: deviations of the profiles, normalized to unit area, from a Gaussian with the same dispersion. Note that a Gaussian has a central amplitude ≈ 0.4. The projected radii are given in units of a. The line styles are the same as in Fig. 1. At $R = 0.05a$ the VP with the greatest deviation at $v = 0$ is that of the model with $\gamma = 0.25$, followed by $\gamma = 0.5$, 0 and 0.75.

to simplify the three-dimensional integral. However, for the isotropic models, $f(\mathscr{E})$, the VP can be calculated by a single integration. For the models of equation (1) this results in

$$l_{\mathrm{i}}(R, v_{\|}) = 4\pi GM \int_R^{r_{\|}} f\left(\Psi(r) - \frac{v_{\|}^2}{2}\right) \frac{r^{1-\gamma}\sqrt{r^2-R^2}}{(r+a)^{3-\gamma}}\,\mathrm{d}r, \qquad (20)$$

where $r_{\|}$ is the radius with $2\Psi(r_{\|}) = v_{\|}^2$, which is given by $r_{\|} = ay(v_{\|}^2/2)/[1 - y(v_{\|}^2/2)]$ with y from equation (7).

In Fig. 3 the deviations of the VPs of the isotropic DFs, normalized to unit area, from a Gaussian with the same dispersion are plotted at the projected radii $R/a = 0.05, 0.5, 5$. In the outer parts, e.g. at $R = 5a$, all models have VPs of a common shape, which is less peaked than a Gaussian but has also less prominent wings (at $v/\sigma \approx 3$). This is the generic form of the VPs in the envelope of an isotropic system with $\rho \propto r^{-4}$ and Keplerian potential at large radii (Gerhard 1993). At $R = 0.5a$ the VPs hardly deviate from a Gaussian. Near the centre, at $R = 0.05a$, the models with $\gamma \geq 7/4$ have VPs that are near-Gaussian, while for $\gamma < 7/4$ the VPs are more peaked. The latter effect can be understood from the fact that, because of the weaker density fall-off along the line of sight for smaller γ, the contribution to the VP of radii larger than R becomes more significant for smaller γ. Stars at those radii contribute at smaller velocities to the VP, creating the peak. The model with $\gamma = 0$, however, is an exception: its intrinsic central velocity dispersion does not go to zero (see above) and therefore its central VP is less peaked than that of the models with $\gamma = 0.25$ or 0.5, as noted in the caption of Fig. 3.

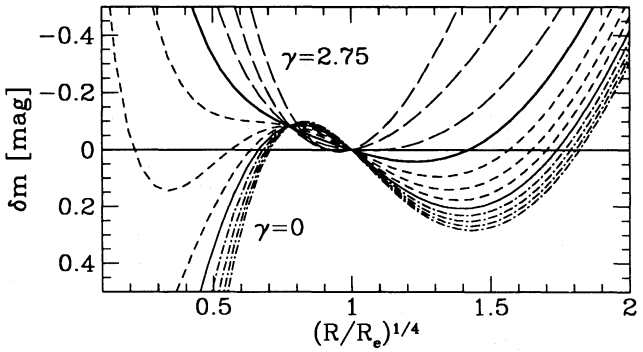

Figure 4. Surface density residuals between the models and the $R^{1/4}$-profile in magnitudes. R_{e} refers separately to the effective radius of each model. The line styles are the same as in Fig. 1.

3 COMPARISON TO THE $R^{1/4}$-MODEL

The surface brightness of many ellipticals and bulges is well represented by the empirical formula

$$I(R) = I_{\mathrm{e}}\, \mathrm{e}^{-7.6692[(R/R_{\mathrm{e}})^{1/4}-1]}, \qquad (21)$$

where the effective radius, R_{e}, and $I_{\mathrm{e}} = I(R_{\mathrm{e}})$ are free parameters (de Vaucouleurs 1948). In this section, the properties of the model with the surface density of equation (21) are compared to those of the models defined in equation (1).

3.1 Surface density

At large radii the models of equation (1) have surface density $\Sigma \propto R^{-3}$, while de Vaucouleurs' formula falls off exponentially. The central surface density of the $R^{1/4}$-profile is finite and falls off like $R^{1/4}$ for very small radii. However, there is a range of intermediate radii over which the models of equation (1) do not differ much from a de Vaucouleurs profile. This can be recognized in Fig. 4, where the residuals to de Vaucouleurs' profile are plotted for various values of γ from 0 to 2.75. Models with $\gamma > 2$ differ significantly from the $R^{1/4}$-profile: they go into the centre more steeply and are flatter in the envelope. Models with $\gamma \leq 2$ have rather small residuals in a radial range around R_{e}. The model with $\gamma = 3/2$ maximizes this range: over nearly four decades in radius it agrees with the de Vaucouleurs profile to within $\simeq 15$ per cent. For $\gamma < 1$ the differences in the residuals are quite small, i.e. these models describe the $R^{1/4}$-profile only slightly less well than does Hernquist's model.

3.2 Energy distributions

The potential and isotropic distribution function for de Vaucouleurs' model are tabulated by Binney (1982). From these the differential mass distribution $N(E)$ can be computed.

In Fig. 5, $f(E)$ and $N(E)$ of the $R^{1/4}$-model are plotted, together with those of the models of equation (1) which have finite $\Psi(0)$. The central potential depths of de Vaucouleurs' model and of the model with $\gamma = 3/2$ are almost identical in units of GM/R_{e}, which means that their intrinsic mass distributions are rather similar. In turn, the effective radii of the two models are comparable in units of $GM/\Psi(0)$ (cf. Fig. 5), while they are smaller for $\gamma > 3/2$ and larger for $\gamma < 3/2$. For this reason those two models compare well in Fig. 5.

Downloaded from https://academic.oup.com/mnras/article/265/1/250/975506 by guest on 20 August 2022

© Royal Astronomical Society • Provided by the NASA Astrophysics Data System

1993MNRAS.265..250D

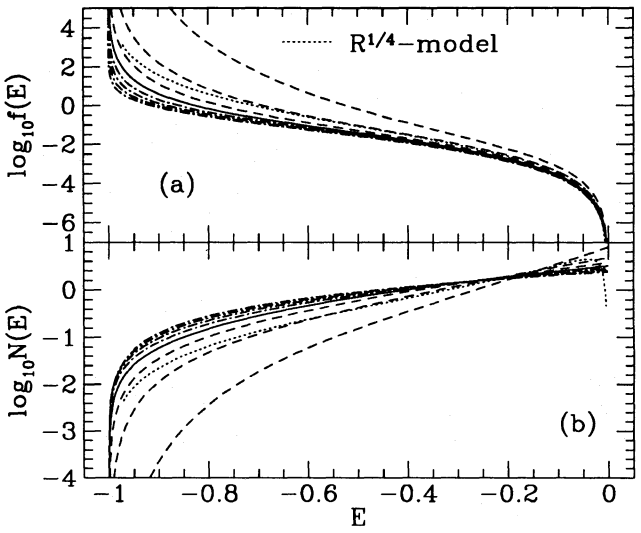

Figure 5. $f(E)$ and $N(E)$ of the models with $\gamma < 2$ and the $R^{1/4}$-profile. Units are such that $G \equiv M \equiv \Psi(0) \equiv 1$. The line styles are the same as in Fig. 1.

4 CONCLUSIONS

A family of spherical mass models has been investigated. The densities are proportional to r^{-4} at large radii and diverge in the centre like $\rho \propto r^{-\gamma}$, where $0 \le \gamma < 3$. Therefore models corresponding to different γ mainly differ in their central parts, out to a few scale radii, where the transition between $r^{-\gamma}$ and r^{-4} occurs, but are very similar to each other in the envelope. The typical behaviour of the scaling quantities, intrinsic and projected, suggests a subdivision into three domains, $0 \le \gamma < 1$, $1 < \gamma < 2$ and $2 < \gamma < 3$, divided by the models with $\gamma = 1$ (Hernquist 1990) and $\gamma = 2$ (Jaffe 1983), respectively.

The models of the first domain, $0 \le \gamma < 1$, are very similar to each other in most properties. They have surface density profiles that are finite in the centre, can hardly be distinguished from a model with a core ($\gamma = 0$), and resemble the de Vaucouleurs profile almost as well as does Hernquist's model. Their projected isotropic velocity dispersion profiles are centrally flat and have a maximum at $r \simeq 0.3 - 0.8$ scale radii, which becomes less prominent for smaller γ. The dynamically isotropic models have central line-of-sight velocity profiles that are more peaked than a Gaussian, while at large radii they are more flat-topped compared to a Gaussian. The latter property is also found for $\gamma > 1$, which is not surprising because the mass models are similar at large radii.

Models with $1 < \gamma < 2$ lie between the two well-known models by Hernquist (1990) and Jaffe (1983). Their surface density profiles have a central $R^{1-\gamma}$-cusp, but nevertheless closely resemble the $R^{1/4}$-profile over a large range in radius around R_e. The projected velocity dispersion profiles of the isotropic models have a maximum close to the centre and dip to zero at $r = 0$. The latter effect is caused by the surface density (zeroth moment) diverging more strongly than the second moment ($\Sigma\sigma^2$). The effects of seeing will cut these singularities to finite values and lead to a non-zero observed central velocity dispersion. The central VPs of the isotropic models are slightly more peaked than a Gaussian, but less so than for models of the first domain.

The third domain, $2 < \gamma < 3$, comprises models that are probably less useful because of some unrealistic properties, such as infinite central potential, diverging central velocity dispersions, and surface density profiles that do not resemble the $R^{1/4}$-profile. The central VPs of the isotropic models are near-Gaussian.

The results on the typical scaling properties at small radii or high binding energies are not restricted to the family of models presented. They hold also for models with an intrinsic cusp but different density profile in the outer parts, as long as (i) the density falls off steeper than r^{-3} at large radii and (ii) the mass-to-light ratio is constant in the centre (no black hole). Exceptions are models with a core, since in these cases the behaviour also depends on the way in which the density falls off from its central value.

Of special interest is the model $\gamma = 3/2$ because (i) it is analytical in all its properties, and (ii) it most closely resembles the de Vaucouleurs model in both distribution function and surface density, where it agrees to within 15 per cent (or 0.15 mag) in the range $0.001 \le R/R_e \le 8$, corresponding to 12 mag in surface density. It is thus the best analytical representation of the $R^{1/4}$-profile known so far.

ACKNOWLEDGMENTS

The author thanks Ortwin E. Gerhard for some helpful discussions and for a critical reading of an early version of this paper. During this work he was supported by SFB 328.

REFERENCES

Bender R., 1990, A&A, 229, 441
Binney J.J., 1982, MNRAS, 200, 951
Binney J.J., Tremaine S., 1987, Galactic Dynamics. Princeton Univ. Press, Princeton (BT)
Ciotti L., 1991, A&A, 249, 99
Crane P., Stiavelli M., 1993, in Danziger I.J., Zeilinger W.W., Kjär K., eds, ESO Proc. No. 45, Structure, Dynamics and Chemical Evolution of Elliptical Galaxies. ESO, Garching, p. 137
de Vaucouleurs G., 1948, Ann. Astrophys., 11, 247
Franx M., Illingworth G.D., 1988, ApJ, 327, L55
Gerhard O.E., 1993, MNRAS, in press
Hénon M., 1959, Ann. Astrophys., 22, 126
Hernquist L., 1990, ApJ, 356, 359
Jaffe W., 1983, MNRAS, 202, 995
Lauer T.R. et al., 1992, AJ, 104, 552
Merritt D., 1985, AJ, 90, 1027
Osipkov L.P., 1979, Pis'ma Astron. Zh., 5, 77
Rix H.W., White S., 1992, MNRAS, 254, 389
van der Marel R.P., Franx M., 1993, ApJ, 407, 525

APPENDIX A: PARTICULAR MODELS

As mentioned in Section 2, most of the model characteristics can be given analytically for some values of γ other than $\gamma = 1$ (Hernquist model) and $\gamma = 2$ (Jaffe model). This appendix deals with $\gamma = 0$ and 3/2.

To simplify the expressions, the dimensionless quantities $x \equiv r/a$, $s \equiv R/a$ and $\mathscr{E} \equiv -E/(GMa^{-1})$ are used.

Downloaded from https://academic.oup.com/mnras/article/265/1/250/975506 by guest on 20 August 2022

© Royal Astronomical Society • Provided by the NASA Astrophysics Data System

1993MNRAS.265..250D

A1 The model $\gamma = 0$

The density profile

$$\rho = \frac{3M}{4\pi}\frac{a}{(r+a)^4} \tag{A1}$$

is the only one among those of equation (1) that intrinsically has a core. However, it is not an isothermal core, since the derivative $\mathrm{d}\rho/\mathrm{d}r$ does not vanish in the centre. For small radii the potential (equation 2) becomes

$$\Phi(r \ll a) = -\frac{GM}{2a}(1 - x^2 + 2x^3 - 3x^4 + 4x^5 \ldots). \tag{A2}$$

The half-mass radius is $r_{1/2} \approx 3.8473a$. Compared to Hénon's (1959) isochrone, which also has $\Phi(0) = -GM/2a$ but contains an isothermal core and has $r_{1/2} \approx 3.0603a$, this model is less centrally concentrated and the r^{-4} density fall-off occurs at larger radii. The dynamically isotropic model has velocity dispersion

$$v_r^2(r) = \frac{GM(1+6r)}{30(r+a)^2}, \tag{A3}$$

with the maximum $v(2/3a)/\sqrt{GM/a} = \sqrt{3/50} \approx 0.24495$. The circular orbit's angular momentum is given as function of energy in equation (10) with

$$y_c(\mathscr{E}) = \frac{2}{3} + \frac{4}{3}\cos\left(\frac{4\pi}{3} + \frac{1}{3}\arccos\frac{54\mathscr{E}-11}{16}\right). \tag{A4}$$

The isotropic DF and the density of states are

$$f(\mathscr{E}) = \frac{3M}{2\pi^3(GMa)^{3/2}}\left(\sqrt{2\mathscr{E}}\frac{3-4\mathscr{E}}{1-2\mathscr{E}} - 3\,\mathrm{arsinh}\sqrt{\frac{2\mathscr{E}}{1-2\mathscr{E}}}\right), \tag{A5}$$

$$g(\mathscr{E}) = 8\pi^2\sqrt{GMa^5}\left[\sqrt{1-2\mathscr{E}}\frac{3-14\mathscr{E}-8\mathscr{E}^2}{12\mathscr{E}^2} - \pi + \frac{1-6\mathscr{E}+16\mathscr{E}^2}{(2\mathscr{E})^{5/2}}\arccos(-\sqrt{1-2\mathscr{E}})\right]. \tag{A6}$$

The anisotropic DF of Osipkov–Merritt type (cf. Section 2) is

$$f_{\mathrm{OM}}(Q) = f(Q) + \frac{a^2}{r_a^2}\frac{3M}{8\pi^3(GMa)^{3/2}} \times \left(4\sqrt{2Q} - 3\,\mathrm{arsinh}\sqrt{\frac{2Q}{1-2Q}}\right) \tag{A7}$$

with $f(Q)$ of equation (A5).

Surface brightness and cumulative surface brightness are

$$\Sigma(R) = \frac{M}{4\pi a^2}\frac{1}{(s^2-1)^3}\left[-2-13s^2+3s^2(4+s^2)X(s)\right], \tag{A8}$$

$$S(R) = \frac{M}{2(s^2-1)^2}[s^2 + 2s^4 - 3s^4X(s)], \tag{A9}$$

where

$$X(s) = \begin{cases} (1-s^2)^{-1/2}\,\mathrm{arcosh}\,s^{-1} & s \le 1 \\ (s^2-1)^{-1/2}\arccos s^{-1} & s \ge 1 \end{cases} \tag{A10}$$

is a continuous function with $X(1) = 1$, the asymptotic expressions of which at $s \to 0, 1, \infty$ are given by Hernquist (1990). The effective radius is $R_e \approx 2.9036a$. The projected velocity dispersions of the isotropic and the circular model are

$$\sigma_{\mathrm{p,i}}^2(R) = \frac{3GM^2}{32\pi a^3\Sigma(R)(s^2-1)^5}\left[\frac{4}{15} + \frac{8}{3}s^2 + \frac{247}{15}s^4 + \frac{32}{15}s^6 - 7s^4(2+s^2)X(s)\right], \tag{A11}$$

$$\sigma_{\mathrm{p,c}}^2(R) = \frac{3GM^2\,s^2}{64\pi a^3\Sigma(R)(s^2-1)^6}\left[\frac{8}{3} + \frac{506}{5}s^2 + \frac{593}{5}s^4 + \frac{128}{15}s^6 - 7s^2(8+20s^2+5s^4)X(s)\right]. \tag{A12}$$

A2 The model $\gamma = 3/2$

The model with mass density

$$\rho = \frac{3M}{8\pi}\frac{a}{r^{3/2}(r+a)^{5/2}} \tag{A13}$$

has a central cusp with a slope intermediate between those of the models of Hernquist and Jaffe, and gives the best representation of the $R^{1/4}$-profile among those of equation (1).

The gravitational potential (equation 2) has a central depth of $-2GM/a$, and the half-mass radius is $r_{1/2} \approx 1.7024a$. The velocity dispersion of the isotropic model is

$$v_r^2(r) = \frac{GM}{a}\sqrt{\frac{x}{x+1}}\left[4x(x+1)^3\ln\frac{x}{x+1} + 1 + \frac{22}{3}x + 10x^2 + 4x^3\right], \tag{A14}$$

which in the centre goes to zero and has the maximum $v_r(r \approx 0.1577a) \approx 0.9576\sqrt{GM/a}$.

The circular orbit's angular momentum is given as function of energy in equation (10) with

$$y_c(\mathscr{E}) = \frac{20}{3}\cos^2\left(\frac{4\pi}{3} + \frac{1}{3}\arccos\left[\sqrt{\frac{27}{125}}(\mathscr{E}-2)\right]\right). \tag{A15}$$

The DF of the isotropic model is

$$f(\mathscr{E}) = \frac{3M}{2(2\pi^2GMa)^{3/2}}\frac{\sqrt{\mathscr{E}}}{(2-\mathscr{E})^4}\left[-\frac{9}{16} - \frac{99}{16}\mathscr{E} + \frac{405}{8}\mathscr{E}^2 - \frac{3705}{56}\mathscr{E}^3 + \frac{561}{14}\mathscr{E}^4 - \frac{181}{14}\mathscr{E}^5 + \frac{15}{7}\mathscr{E}^6 - \frac{\mathscr{E}^7}{7} + \frac{3(3+32\mathscr{E}-8\mathscr{E}^2)}{8\sqrt{\mathscr{E}(2-\mathscr{E})}}\arcsin\sqrt{\mathscr{E}/2}\right]. \tag{A16}$$

Equation 13 for the density of states can be rationalized, which yields

$$g(\mathscr{E}) = 128\pi^2\sqrt{GMa^5}\int_0^{\sqrt{1-\mathscr{E}/2}}\frac{(1-\mathscr{E}/2-t^2)^5t^2\,\mathrm{d}t}{[1-(1-\mathscr{E}/2-t^2)^2]^4}; \tag{A17}$$

this integral can be done analytically but it is relatively complicated and much easier to compute numerically. The anisotropic DF of Osipkov–Merritt type (cf. Section 2) is

$$f_{\mathrm{OM}}(Q) = f(Q) + \frac{a^2}{r_a^2}\frac{3M\sqrt{Q}}{2(2\pi^2GMa)^{3/2}}\left[(1-Q)^2 - \frac{Q^3}{7}\right], \tag{A18}$$

with $f(Q)$ of equation (A16).

The surface density can be expressed in terms of incomplete elliptic integrals of the first and second kind:

$$\Sigma(R) = \frac{M}{\pi a^2}\left[\frac{s^2-5}{2(s^2-1)^2} + \frac{s^2-3/2}{\sqrt{s}(s+1)^{5/2}(s-1)^2}F\left(\frac{\pi}{4}, \sqrt{\frac{2}{s+1}}\right)\right. \tag{A19}$$

Downloaded from https://academic.oup.com/mnras/article/265/1/250/975506 by guest on 20 August 2022

© Royal Astronomical Society • Provided by the NASA Astrophysics Data System

1993MNRAS.265..250D

$$+\frac{\sqrt{s}(3-s^2)}{(s+1)^{3/2}(s-1)^2}\,E\left(\frac{\pi}{4},\sqrt{\frac{2}{s+1}}\right)\Bigg].$$

The effective radius is $R_e \approx 1.2757a$.

The projected velocity dispersions of the isotropic model and of the model containing only circular orbits are

$$\sigma^2_{\rm p,i}(R) = \frac{GM^2}{a^3\Sigma(R)}\left[\frac{3s}{2} - \frac{24s^4-44s^2+17}{8\pi(s^2-1)^2} + \frac{3(8s^6-20s^4+15s^2-2)}{8\pi(s^2-1)^2}X(s)\right], \tag{A20}$$

$$\sigma^2_{\rm p,c}(R) = \frac{GM^2}{a^3\Sigma(R)}\left[\frac{24s^6-68s^4+65s^2-6}{16\pi(s^2-1)^3} - \frac{3s}{4} + \frac{3(8s^6-28s^4+35s^2-20)}{16\pi(s^2-1)^3}X(s)\right]. \tag{A21}$$

APPENDIX B: NUMERICAL INTEGRATIONS

For the numerical calculation of surface density, cumulative surface density and projected velocity dispersions, the formulæ given in Section 2 are not very useful because of infinite integration intervals and singularities of the integrands. With the substitution

$$t = \sqrt{\frac{r}{r+a}(s+1) - s}, \qquad s \equiv R/a, \tag{B1}$$

these problems disappear, and the quantities can easily be computed using standard routines for numerical quadrature. The integrals then become

$$\frac{\Sigma(R)}{Ma^{-2}} = \frac{3-\gamma}{\pi(s+1)^{7/2-\gamma}} \times \int_0^1 \frac{(s+t^2)^{1-\gamma}(1-t^2)^2\,{\rm d}t}{\sqrt{2s+(1-s)t^2}}, \tag{B2}$$

$$\frac{S(R)}{M} = 1 - \frac{2(3-\gamma)}{(s+1)^{5/2-\gamma}}\int_0^1 (s+t^2)^{1-\gamma}t^2 \times\sqrt{2s+(1-s)t^2}\,{\rm d}t, \tag{B3}$$

$$\frac{\Sigma(R)\sigma^2_{\rm p,i}(R)}{GMa^{-3}} = \frac{3-\gamma}{\pi(s+1)^{11/2-2\gamma}}\int_0^1 (s+t^2)^{1-2\gamma} \times(1-t^2)^3t^2\sqrt{2s+(1-s)t^2}\,{\rm d}t, \tag{B4}$$

$$\frac{\Sigma(R)\sigma^2_{\rm p,c}(R)}{GMa^{-3}} = \frac{(3-\gamma)s^2}{2\pi(s+1)^{13/2-2\gamma}} \times \int_0^1 \frac{(s+t^2)^{1-2\gamma}(1-t^2)^5\,{\rm d}t}{\sqrt{2s+(1-s)t^2}}. \tag{B5}$$

This paper has been produced using the Blackwell Scientific Publications LaTeX style file.

Downloaded from https://academic.oup.com/mnras/article/265/1/250/975506 by guest on 20 August 2022

© Royal Astronomical Society • Provided by the NASA Astrophysics Data System